SPECIAL
Land–Atmosphere Exchanges of Energy and Water
COLLECTION

Surface Skin Temperature and the Interplay between Sensible and Ground Heat Fluxes over Arid Regions

XUBIN ZENG AND ZHUO WANG

Department of Atmospheric Sciences, The University of Arizona, Tucson, Arizona

AIHUI WANG

Institute of Atmospheric Physics, Chinese Academy of Sciences, Beijing, China

(Manuscript received 4 September 2011, in final form 1 January 2012)

ABSTRACT

Over arid regions, two community land models [Noah and Community Land Model (CLM)] still have difficulty in realistically simulating the diurnal cycle of surface skin temperature. Based on theoretical arguments and synthesis of previous observational and modeling efforts, three revisions are developed here to address this issue. The revision of the coefficients in computing roughness length for heat significantly reduces the underestimate of daytime skin temperature but has a negligible effect on nighttime skin temperature. The constraints of the minimum friction velocity and soil thermal conductivity help improve nighttime skin temperature under weak wind and dry soil conditions. These results are robust in both Noah and CLM, as well as in Noah, with 4 versus 10 soil layers based on in situ data at the Desert Rock site in Nevada with a monthly averaged diurnal amplitude of 31.7 K and the Gaize site over Tibet, China, with an amplitude of 44.6 K. While these revisions can be directly applied to CLM or other land models with subgrid tiles (including bare soil), suggestions are also made on their application to Noah and other land models that treat bare soil and vegetated area together in a model grid cell. It is suggested that the challenging issue of measuring and simulating surface sensible heat flux under stable conditions should be treated as a land–atmosphere coupled issue, involving the interplay of ground and sensible heat fluxes in balancing the net radiation over arid regions, rather than as an atmospheric turbulence issue alone. The implications of such a coupling perspective are also discussed.

1. Introduction

Land–atmosphere interaction plays an important role in weather, climate, and global/regional environmental change. For this reason, various international programs have been established in the past three decades to address the relevant scientific issues, such as the Global Energy and Water Cycle Experiment (GEWEX; http://www.gewex.org), the (earlier) Biospheric Aspects of the Hydrological Cycle (BASC; Kabat et al. 2004), and (its successor) integrated Land Ecosystem–Atmosphere Process Study (iLEAPS; http://www.ileaps.org). With individual and coordinated efforts, significant progress has been made in this area (e.g., Sellers et al. 1997; Zeng et al. 2002; Seneviratne et al. 2006; Koster et al. 2006; Xue et al. 2010; Shuttleworth 2011). However, several outstanding observational and modeling issues remain to be resolved, such as the lack of energy balance in flux tower measurements (e.g., Baldocchi et al. 2001) and the difficulty of land models and reanalysis in realistically simulating or producing surface fluxes and skin temperature (e.g., Jiménez et al. 2011; Decker et al. 2012). Skin temperature (T_s) plays a significant role in the land surface energy balance and is also widely available from remote sensing for model evaluation and data assimilation (e.g., Jin et al. 1997; Reichle et al. 2010).

Over arid and semiarid regions that represent one-third of the global land, the vegetation evapotranspiration and the closely coupled water–carbon cycle play a minor role in the surface energy balance. Despite this simplification, both offline land models and land–atmosphere coupled models still have difficulty in realistically simulating or predicting T_s (Chen et al. 2010; Zheng et al. 2012). A

Corresponding author address: Xubin Zeng, Department of Atmospheric Sciences, 1118 E. 4th St., The University of Arizona, Tucson, AZ 85721.
E-mail: xubin@atmo.arizona.edu

DOI: 10.1175/JHM-D-11-0117.1

© 2012 American Meteorological Society

possible solution from these studies for improving the daytime T_s simulation is to revise the formulation for computing roughness length for heat (z_{oh}). The question is, how robust are such z_{oh} formulations with respect to different land models and different elevations?

Such formulations, however, have a minimal effect on nighttime T_s. There are two questions relevant to the nighttime T_s and the interplay between sensible and ground heat fluxes: How can the sensible heat flux be constrained under stable (atmospheric stratification) conditions in measurements and modeling? And how can the computation of ground heat flux be constrained in land modeling?

The goal of this study is to improve the modeling of surface skin temperature diurnal cycle over arid regions by addressing these three questions. Two community land models will be used: the Noah land model (Ek et al. 2003; Chen and Dudhia 2001) as used in the National Centers for Environmental Prediction (NCEP) regional and global weather forecasting models as well as in the National Center for Atmospheric Research (NCAR) Weather Research and Forecasting (WRF) model, and the Community Land Model (CLM3.5) (Oleson et al. 2008) as used in the NCAR Earth System Model. While this study focuses on arid regions, relevant revisions will be formulated for all vegetation types with different fractional vegetation cover so that these revisions can be further tested and evaluated by the community in the future.

Section 2 elaborates on these three questions and suggests preliminary solutions based on theoretical arguments and synthesis of previous observational and modeling efforts. Section 3 discusses sensitivity test results using observational data at two barren sites (one over the western United States and the other over Tibet, China), and discusses the potential applicability of these revisions to different vegetation types. Section 4 gives the conclusions.

2. Theoretical framework

a. Governing equations

Over land surface, the net radiative flux (R_{net}) (with downward fluxes positive) is balanced by the sensible heat (SH), latent heat (LH), and ground heat (G) fluxes (with fluxes away from surface positive):

$$R_{net} = SW_d(1-\alpha) + \epsilon(LW_d - \sigma T_s^4) = SH + LH + G, \tag{1}$$

where SW_d and LW_d are downward shortwave and longwave fluxes, α is surface albedo, ϵ is surface emissivity, $\sigma = 5.67 \times 10^{-8}$ W m^{-2} K^{-4} is the Stefan–Boltzmann constant, and T_s is the surface skin temperature. Over arid regions, LH is much smaller than SH in magnitude and can be omitted (but it is still fully considered in Noah and CLM simulations here). The ground heat flux is

$$G = K_{soil}\frac{T_{soil} - T_s}{\Delta z}, \tag{2}$$

where K_{soil} is the soil thermal conductivity, which depends on soil composition, porosity, and moisture, and T_{soil} is the soil temperature at depth Δz for observational measurements. In the Noah land model, T_{soil} represents the average temperature of the top soil layer, and Δz represents the distance from surface to the middle of the top soil layer.

The sensible heat flux (e.g., in CLM and Noah) can be expressed using aerodynamic resistance (R_{ah}) and surface resistance (R_{ss}) (Zeng and Dickinson 1998):

$$SH = -\rho C_p u_* \theta_* = \rho C_p \frac{T_s - \theta_a}{R_{ah} + R_{ss}}, \tag{3}$$

where ρ is the air density, C_p is the air heat capacity, $\theta_a = T_a + gz/C_p$ is the near-surface locally defined potential temperature with T_a being the surface air temperature, g is gravity, z is the measurement height, and the friction velocity u_* and temperature scaling (θ_*) are

$$u_* = kU_a \Big/ \left[\ln\frac{z}{z_{om}} - \Psi_m\left(\frac{z}{L}\right) + \Psi_m\left(\frac{z_{om}}{L}\right)\right], \quad \text{and} \tag{4}$$

$$\theta_* = k(\theta_a - T_s) \Big/ \left[\ln\frac{z}{z_{oh}} - \Psi_h\left(\frac{z}{L}\right) + \Psi_h\left(\frac{z_{oh}}{L}\right)\right], \tag{5}$$

where $k = 0.4$ is the Von Kármán constant, U_a is the near-surface atmospheric wind speed, z_{om} is the roughness for momentum, z_{oh} is the roughness length for heat, and Ψ_m and Ψ_h are stability functions of the Monin-Obukhov length L:

$$L = \frac{\theta u_*^2}{kg\theta_*}. \tag{6}$$

For instance, these functions as used in CLM are discussed in Zeng et al. (1998). The aerodynamic and surface resistances in (3) are

$$R_{ah} = \left[\ln\frac{z}{z_{om}} - \Psi_m\left(\frac{z}{L}\right) + \Psi_m\left(\frac{z_{om}}{L}\right)\right] \times \left[\ln\frac{z}{z_{om}} - \Psi_h\left(\frac{z}{L}\right) + \Psi_h\left(\frac{z_{om}}{L}\right)\right] \Big/ (k^2 U_a), \quad \text{and} \tag{7}$$

$$R_{ss} = \ln(z_{om}/z_{oh})/(ku_*), \quad (8)$$

where the ratio of roughness lengths is parameterized as

$$\ln(z_{om}/z_{oh}) = a\left(\frac{u_* z_{om}}{\nu}\right)^b, \quad (9)$$

where $\nu = 1.5 \times 10^{-5}$ m^2 s^{-1} is the molecular viscosity, $b = 0.45$ in CLM and 0.5 in Noah, and $a = 0.13$ in CLM and 0.04 ($=0.4C_{zil} = 0.4 \times 0.1$) in Noah (Ek et al. 2003). In general, z_{om} is greater than z_{oh} because the momentum transfer in the surface sublayer is affected by both the molecular diffusion and pressure fluctuations (particularly around bluff elements) while the heat transfer is affected by the molecular diffusion only (Zeng and Dickinson 1998).

To illustrate the diurnal cycle of the relative importance of SH versus G, we use the observational data when T_s is close to its maximum (in early afternoon) and minimum (in early morning) on 5 May 1998 at the Gaize site (32.30°N, 84.05°E; elevation 4416 m) over Tibet (see section 3a for more details). In the early afternoon (0700 UTC 5 May 1998), observed $R_{net} = 470$ W m^{-2} and soil heat flux at 0.025-m depth $G_{0.025\ m} = 125$ W m^{-2} (downward). While G and SH are not directly measured, G is roughly 10%–20% higher than $G_{0.025\ m}$ (138–150 W m^{-2}) (as estimated by Noah and CLM modeling at this hour) and SH can be estimated as $(R_{net} - G) = 320$–332 W m^{-2} (upward). Obviously SH is larger than G under an unstable (atmospheric stratification) condition, as is well recognized (e.g., Garratt 1992). Separately, SH can also be computed from (3)–(9) using observed T_a, T_s, and U_a. For $a = 0.4 \times 0.1 = 0.04$ and $b = 0.5$ (as used in Noah), SH (=762 W m^{-2}) is unrealistic as it is much larger than the above observationally inferred value and it is even higher than R_{net} itself. Furthermore, R_{ah} (=23.2 s m^{-1}) is much larger than R_{ss} (=3.8 s m^{-1}). Similarly, for $a = 0.13$ and $b = 0.45$ (as used in CLM), SH (=610 W m^{-2}) is also too large, and R_{ss} is too small compared with R_{ah}. The conclusion that both Noah and CLM overestimate the daytime SH is valid even if the observationally inferred $(R_{net} - G)$ contains an uncertainty of 10%–20%. It is also clear from (3) that the simulation of SH can be improved by increasing R_{ss} in (8) [i.e., by increasing the coefficient a in (9)], which will be discussed in section 2b. The question is, can the same formulation (9) with the same coefficients a and b be used for two different land models (Noah and CLM)?

In the early morning (2200 UTC 4 May 1998), observed R_{net} (effectively the net longwave radiative flux) = -112 W m^{-2} and $G_{0.025\ m} = -55$ W m^{-2} (upward). The quantity G is roughly 10%–20% higher in magnitude than $G_{0.025\ m}$ (-61 to -66 W m^{-2}) (as estimated by Noah and CLM modeling at this hour), and SH can be estimated as $(R_{net} - G) = -46$ to -51 W m^{-2} (downward). With the a and b values in Noah or CLM, (3)–(9) can also be solved to obtain SH of around -0.4 W m^{-2}, which is substantially lower in magnitude than the above observationally inferred value. Furthermore, u_* is also very small (less than 0.01 m s^{-1}). The conclusion that both Noah and CLM underestimate the nighttime SH in magnitude is valid even if the observationally inferred $(R_{net} - G)$ contains an uncertainty of 10%–20%. In these calculations, because z/L is greater than 2, it is taken as 2 (as constrained in CLM). If the maximum z/L is taken as 1 (as constrained in Noah), the computed SH is still very close to 0 (-0.8 W m^{-2}). The question is, how can the nighttime SH be increased in magnitude under very stable conditions? In contrast to the early afternoon situation when R_{ss} is important, R_{ah} is more than an order of magnitude greater than R_{ss} (and hence R_{ss} is not so important) in the early morning.

b. Proposed revisions

The importance of z_{oh} in simulating surface temperature and fluxes over bare soil is widely recognized (e.g., Zeng and Dickinson 1998; Mitchell et al. 2004; LeMone et al. 2008). Chen et al. (2010) evaluated several different formulations, including (9) with a and b used in CLM and Noah, and found that the z_{oh} formulation as a function of u_* and θ_* from Yang et al. (2008) performed best. Separately, Chen and Zhang (2009) suggested computing a in (9) as a function of canopy height.

Parallel to these efforts, our studies in recent years suggested taking $a = 0.4 \times 0.8 = 0.32$ and $b = 0.5$ in (9) for the computation of z_{oh} (Zheng et al. 2012), and these values were implemented in the NCEP Global Forecast System (GFS) in May 2011. Indeed, with these values, the early afternoon SH at the Gaize site would be 348 W m^{-2}, which is much closer to the observationally inferred value of 320–332 W m^{-2}. Using $a = 0.36$ would produce even better SH of 323 W m^{-2}. The increase of a has a negligible effect on SH in the early morning.

The use of $a = 0.36$ is consistent with the value (0.365) from Chen and Zhang (2009) if the canopy height of bare soil is taken as $10z_{om}$ with $z_{om} = 0.01$ m. The SH results with $a = 0.36$ are also consistent with those using the z_{oh} formulation as a function of both u_* and θ_* in Yang et al. (2008) (with SH = 323 W m^{-2} in the early afternoon and -0.5 W m^{-2} in the early morning at the Gaize site). However, R_{ss} based on the z_{oh} formulation in Yang et al. (2008) becomes negative in the early morning, which is difficult to interpret physically, as was also recognized by Yang et al. (2008).

Since there is no strong justification for the exact value of b (0.45 in CLM versus 0.5 in Noah), we use $b = 0.5$

along with $a = 0.4 \times 0.9 = 0.36$ for both CLM and Noah in the sensitivity tests in section 3.

The second issue raised in section 2a is the very small SH (~0) computed from (3) to (9) under very stable conditions, which is a well-recognized problem in turbulence research (Fernando and Weil 2010; Baklanov et al. 2011). Furthermore, under such conditions, eddy-correlation measurements of SH are also very small, and such underestimates of SH are widely recognized in the flux tower measurement community (e.g., Goulden et al. 1996; Gu et al. 2005). If SH is close to zero, the atmospheric boundary layer would be decoupled from the land surface. For land–atmosphere coupled modeling, this would degrade the model results in the atmospheric boundary layer (Beljaars and Viterbo 1998).

On the other hand, SH should not be close to zero under stable conditions from three lines of arguments. First, as discussed in section 2a, based on surface energy balance, SH should be close to the observationally inferred ($R_{\mathrm{net}} - G$) of −46 to −51 W m^{-2} and hence is far from 0 at night over arid regions. This is true even if we consider various uncertainties: an uncertainty of 10%–20% in ($R_{\mathrm{net}} - G$) or an uncertainty of 10 W m^{-2} in both R_{net} and G, the uncertainty of neglecting LH (probably within a few W m^{-2} under very stable conditions over arid regions), and the uncertainty associated with the representativeness of soil heat flux measurements (to be further discussed in section 3b). Second, based on the assumption of local scaling in the very stable atmospheric boundary layer, SH is related to the wind speed (U_g) at the top of the atmospheric boundary layer (Garratt 1992). Even if the near-surface wind is nearly 0 (under very stable conditions), U_g may not be 0. Assuming $U_g \sim$ 5–10 m s^{-1}, SH would be ~−10 to −40 W m^{-2} (Garratt 1992, 168–169). Finally even over a relatively flat surface with light synoptic winds, there are usually a lot of transient phenomena (e.g., waves, density currents, etc.) that can lead to bursts of heat flux so that the average SH is not zero (e.g., Mahrt 2010).

A main reason for the above discrepancies is that, when the surface layer is very stable (e.g., for z/L greater than 1–2), the boundary layer depth is too shallow, and the measurement height z is above the surface layer where the similarity theory [which is the basis of (3)–(9)] is valid. For instance, for the early morning case in section 2a, z/L is greater than 2, and we can roughly estimate the boundary layer height to be a few meters only based on Garratt (1992, p. 166).

A practical solution for this problem is to constrain u_* to be above a minimum value ($u_{*\mathrm{min}}$). This approach is widely used to adjust the eddy-correlation flux measurements from towers (Gu et al. 2005), and $u_{*\mathrm{min}}$ is around 0.17–0.22 m s^{-1} over forests based on literature survey. In the different versions of WRF/Noah, $u_{*\mathrm{min}}$ is taken as 0.07 m s^{-1}. An alternative way is to adjust the stability functions in (4)–(5) (Beljaars and Viterbo 1998). Under weak wind, very unstable conditions, the boundary layer scaling has been used to treat the nonzero flux (e.g., Zeng et al. 1998). However, such a scaling has not been developed for global applications under very stable conditions.

Even though the physical justification for the $u_{*\mathrm{min}}$ approach is still not satisfactory, we take this approach here for two reasons: it is widely used by the flux tower measurement community and by some land models (e.g., WRF/Noah), and it is easy to implement. Furthermore, since SH is proportional to ρu_* in (3), we should constrain ρu_* rather than u_* itself. To be consistent with the $u_{*\mathrm{min}}$ values used by the modeling and observational communities, our suggested formulation is

$$u_{*\mathrm{min}} = 0.07\,\frac{\rho_0}{\rho}\left(\frac{z_{\mathrm{om}}}{z_{\mathrm{og}}}\right)^{0.18}, \tag{10}$$

where the density at the sea level ρ_0 is taken as 1.22 kg m^{-3} (with the mean temperature of 15°C), the bare soil roughness length z_{og} is taken as 0.01 m, and the exponent of 0.18 ensures that $u_{*\mathrm{min}}$ converges to 0.07 m s^{-1} over bare soil (consistent with that in WRF/Noah) and 0.16–0.21 m s^{-1} for forests (consistent with those used by the observational community). This constraint should be used for stable conditions only, even though u_* under unstable conditions is usually greater than the above $u_{*\mathrm{min}}$.

For the Gaize site in section 2a, $u_{*\mathrm{min}}$ is about 0.11 m s^{-1} for the early morning case, and its use would change SH from −0.4 to −16 W m^{-2}, which is better but still too small in magnitude compared with the observationally inferred value of −46 to −51 W m^{-2}. Only for $u_{*\mathrm{min}}$ = 0.28 m s^{-1} does SH (of −47 W m^{-2}) become consistent with the observationally inferred value. Since $u_{*\mathrm{min}}$ of 0.28 m s^{-1} cannot be justified based on the above literature survey, we have to address the computation of G in (2), which would affect the computation of T_s and SH through surface energy balance in (1). This is the last issue raised in section 1.

While the expression (2) is relatively simple, the determination of K_{soil} is far from straightforward for several reasons. Even though global 10-km and U.S. 1-km soil data are available, there are substantial horizontal heterogeneities in soil properties. Therefore, soil texture data used in any land models (including CLM and Noah) contain large uncertainties. Furthermore, pedotransfer functions used to calculate K_{soil} and soil hydraulic properties from soil texture are highly uncertain (e.g., Gutmann and Small 2007). Partly for these reasons,

a single soil texture is used in the operational model at the European Centre for Medium-Range Weather Forecasts (ECMWF). Furthermore, the computation of K_{soil} is different in different land models. For instance, while Noah uses soil texture types, CLM uses percentages of sand and clay to quantify soil texture in the computation of K_{soil} and other soil variables.

Because of the strong, nonlinear soil temperature gradient with depth near the surface, the linearization used in (2) also introduces some errors in the G computation. For instance, Δz is reduced in CLM (Oleson et al. 2010) to more reasonably simulate surface skin temperature. In the ECMWF model (http://www.ecmwf.int/research/ifsdocs/CY31r1/PHYSICS/IFSPart4.pdf), with the top soil layer thickness of 0.07 m [or Δz of 0.035 m in (2)], $K_{soil}/\Delta z$ is taken as 15 W m^{-2} K^{-1} in the surface energy balance computation.

Our suggestion is to constrain the minimum K_{soil} (i.e., $K_{soil,min}$) to be 0.75 W m^{-1} K^{-1} in Noah (with the top soil layer of 0.1 m or Δz of 0.05 m) so that $K_{soil}/\Delta z$ = 15 W m^{-2} K^{-1}, in agreement with that in the ECMWF model. The same $K_{soil,min}$ is proposed for the top soil layer only in Noah and CLM. This constraint is needed for very dry soil only, as K_{soil} is generally greater than $K_{soil,min}$ for soil that is not so dry—for example, for sandy clay soil at the wilting point (with volumetric soil moisture of 0.1) in Noah.

3. Results

a. Data and model descriptions

Two arid sites with different elevations are used: Desert Rock (36.63°N, 116.02°W; elevation 1007 m) in Nevada as part of the surface radiation network (http://www.srrb.noaa.gov/surfrad/) and Gaize (32.30°N, 84.05°E; elevation 4416 m) over Tibet, China, during the GEWEX Asian Monsoon Experiment—Tibet (GAME-Tibet; http://monsoon.t.u-tokyo.ac.jp/tibet/). Observational data of near-surface air temperature, wind, humidity, surface precipitation (which is zero during the modeling period), and downward shortwave and longwave radiation fluxes for May 1998 (at Gaize) and July 2007 (at Desert Rock) are used. Since the diurnal cycle of observed and simulated quantities at these arid sites is very similar from day to day, monthly simulations are sufficient. For the same reason, only the diurnal cycle averaged from days 3–31 May 1998 (or 3–31 July 2007) is emphasized (i.e., the model simulations in the first two days are omitted). Figure 1 shows that while the averaged diurnal amplitude is 31.7°C at Desert Rock, it is as large as 44.6°C at Gaize.

Besides the observational data used for driving land models, net radiation flux and T_s data are available at both sites for model validation. Soil heat flux data at 0.025- and 0.075-m depth are also available at Gaize. Skin temperature (T_s) is obtained from observed upward and down longwave radiation fluxes as well as surface emissivity at Desert Rock and was directly measured at Gaize using a thermometer, with half of the sensor buried in the soil and half exposed to the air (Chen et al. 2010). The T_s uncertainty is 2°–3°C. While all T_s data at Desert Rock are of good quality, the T_s data at Gaize are found to be inconsistent with other observed variables for some hours of the 11 days during 3–31 May 1998 (e.g., increasing T_s associated with abrupt decrease of downward solar flux during the day). Therefore only the remaining 18 days at Gaize (when all forcing and validation data are consistent in our data evaluations) are used for model evaluations in Figs. 1–4.

Model-simulated and observed fluxes are based on 30-min averages and hence can be directly compared. In contrast, while the measured T_s represents a 30-min average, model-simulated T_s represents the instantaneous value. Therefore, the observed T_s values centered at two adjacent periods (e.g., at 0715 and 0745 UTC) are averaged for comparison with the model-simulated T_s (e.g., at 0730 UTC). Such a subtle difference is important here because of the huge diurnal cycle of T_s in Fig. 1.

As mentioned earlier, two community land models (CLM and Noah) are used here. The turbulence scheme in Noah (Ek et al. 2003) and CLM (Oleson et al. 2008) is similar. Noah has four soil layers with the top layer of 0.1 m, and computes T_s separately. In contrast, CLM has 10 soil layers with the top 3 layers of 0.0175, 0.0276, and 0.0455 m in thickness, respectively. The temperature of the top thin layer is taken as T_s. Since the former would have somewhat reduced diurnal amplitude compared with the latter, the heat capacity of the top layer is adjusted in CLM [by reducing Δz in the computation of G in (2)] (Oleson et al. 2010). In other words, T_s and T_{soil} in (2) denote the temperature for the first and second layers in CLM, respectively.

As mentioned earlier, while Noah computes soil thermal and hydraulic properties based on soil texture types (Ek et al. 2003), CLM does the computations based on sand and clay percentages. Noah prescribes surface albedos that are variable seasonally and spatially, while CLM computes surface albedos through two-stream radiative transfer of diffuse and direct radiation at visible and near-infrared bands. Over bare soil, the effect of soil moisture on surface albedo is also considered in CLM (Wang et al. 2005). In the Noah version 2.7.1 (as used in the NCEP global forecasting model), surface emissivity is taken as 1, while it is generally variable in CLM.

In the sensitivity tests here, bare soil is assumed at both sites based on the metadata about the sites and

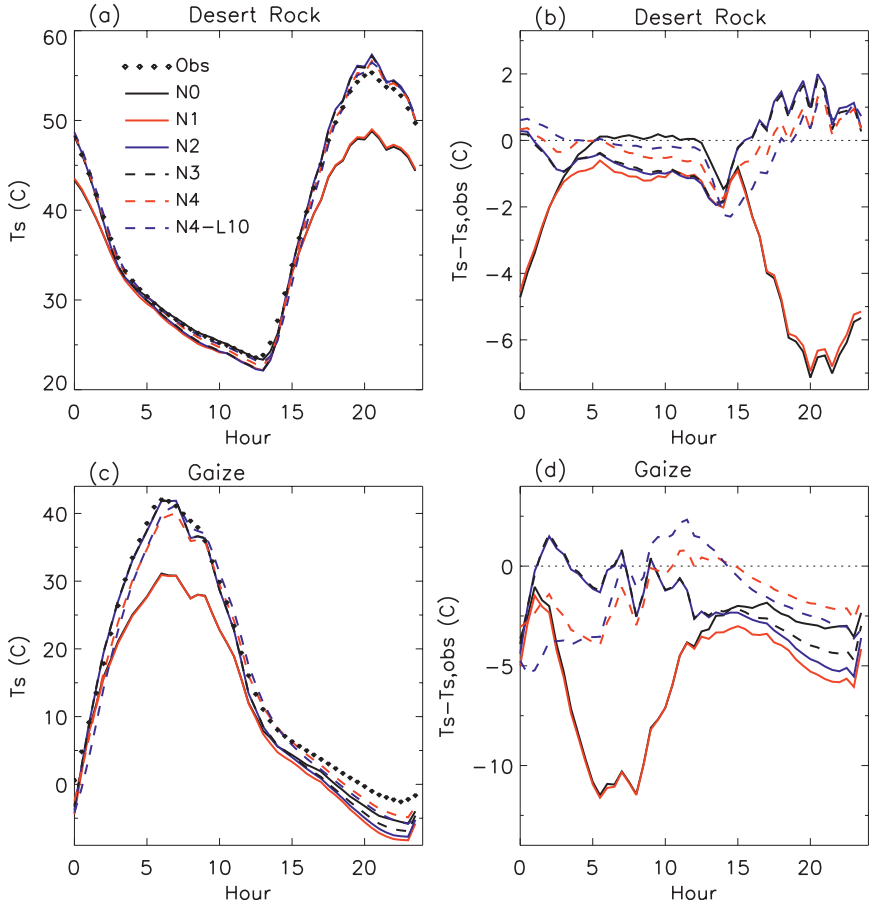

FIG. 1. Observed and Noah-simulated surface skin temperature (T_s) averaged (a) from 3 to 31 Jul 2007 at Desert Rock (36.63°N, 116.02°W; elevation 1007 m) in Nevada and (c) from 18 days during 3–31 May 1998 at Gaize (32.30°N, 84.05°E; elevation 4416 m) over Tibet, China. The differences between (b) simulated and (d) observed T_s. Model sensitivity tests are explained in Table 1 and section 3b.

prior modeling studies. The Gaize site contains dry and thin weedlike plant (with canopy height less than 0.05 m) in May (before the rainy season), and was taken as bare soil in Chen et al. (2010) and Yang et al. (2008). The Desert Rock site also contains some dry shrubs in July, and the green vegetation fraction in July for the GFS grid cell covering this site is 0.03 with the Noah vegetation type 11 (bare soil) in the NCEP global forecasting model (Zheng et al. 2012). Default surface emissivity is used (i.e., 1.0 in Noah and 0.96 in CLM). Soil texture is sandy clay at Gaize and sandy loam at Desert Rock. Observed surface albedo is used in Noah (0.28 at Gaize and 0.22 at Desert Rock). Appropriate soil color is also used in CLM so that the average albedo is consistent with the observed value. Initial volumetric soil moisture (of 0.05) and soil temperature are prescribed from observations at Gaize. They are prescribed from multiyear offline CLM simulations at Desert Rock with the initial volumetric soil moisture of 0.08 in the top 0.1 m; as such observations are not available.

Besides the standard Noah simulation with four soil layers, we also ran Noah with 10 soil layers with layer thicknesses (from top to bottom layers) of 0.02, 0.03, 0.06, 0.08, 0.12, 0.20, 0.34, 0.55, 0.91, and 1.51 m, which are similar to those in CLM. However, since the first soil layer temperature is used to represent T_s in CLM (which may be fine for a thin layer), we decided not to run CLM with the four layers as those in Noah.

b. *Sensitivity tests*

Figure 1 shows that the default Noah simulation (denoted as N0 in Table 1) significantly underestimates early afternoon T_s by about 7°C at Desert Rock and 12°C at Gaize. Nighttime results seem to be very good, consistent with those in Chen et al. (2010). However, our further analysis indicates that the nighttime results are

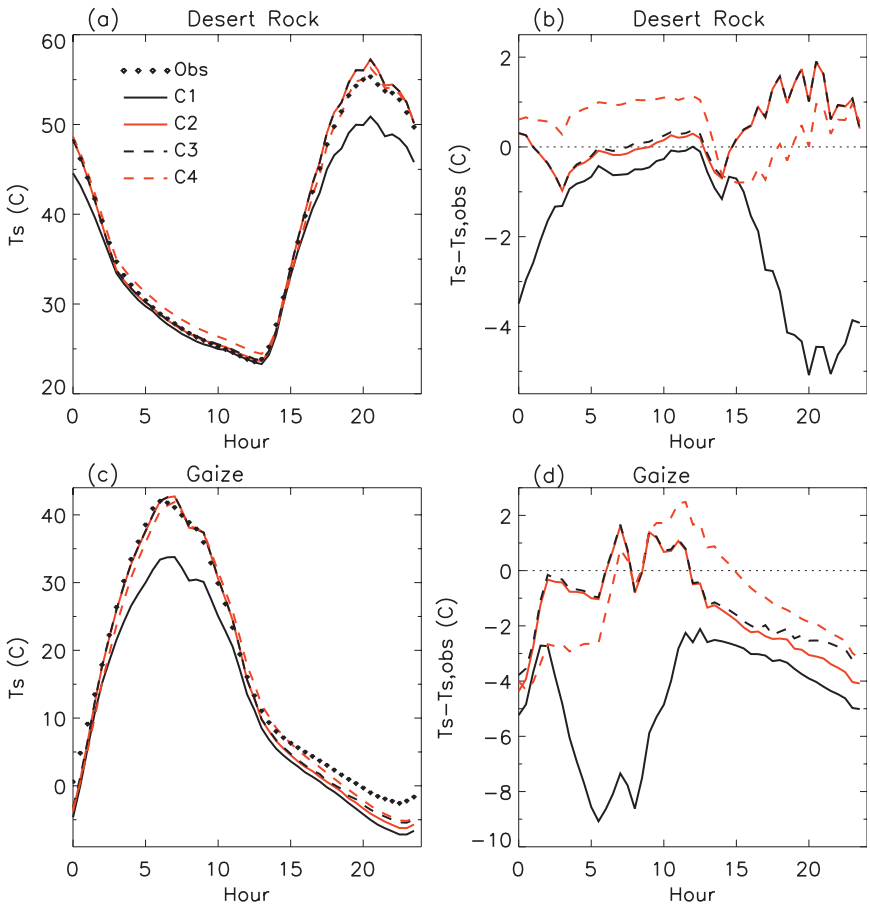

FIG. 2. As in Fig. 1 except using CLM.

spurious because of the lack of convergence in the iterative turbulence computation of (3)–(9) in Noah. Specifically, from Noah version 2.7.1 to the most recent version 3.2, the prescribed initial values used in the iteration along with the maximum iteration number of 5 lead to spuriously high u_* and downward SH values under stable conditions, which, in turn, lead to a higher T_s. This issue was first identified under snow conditions in our recent study (Wang et al. 2010). One simple solution is to increase the maximum iteration number from 5 to 30, and the Noah simulation is denoted as N1 in Table 1 (with N1 referred to as the control Noah simulation hereafter). Figure 1 indicates that N1 underestimates the nighttime T_s by about 1°C at Desert Rock (Figs. 1a,b) and 3°–6°C at Gaize (Figs. 1c,d). In contrast, this correction has a negligible effect on the daytime T_s. It is expected that this correction would affect the nighttime T_s results from Noah offline simulations over arid regions in almost all previous studies (e.g., Chen et al. 2010). It remains to be studied if this correction affects the results over arid regions from land–atmosphere coupled modeling (e.g., in WRF/Noah or GFS/Noah).

N2 in Table 1 represents the Noah simulation (N1) with the coefficient a in (9) increased from 0.04 to 0.36 (or C_{zil}, as widely used in the Noah literature, increased from 0.1 to 0.9) while $b = 0.5$ remains the same. Figure 1 shows that the daytime T_s simulation is significantly improved with the maximum bias of 2°C (versus −7°C in N1) at Desert Rock (Fig. 1b) and of 2°C (versus −12°C in N1) at Gaize (Fig. 1d). Nighttime T_s simulation is only slightly improved at both sites. These results are consistent with those in Zheng et al. (2012).

The N3 in Table 1 denotes N2 along with the constraint on the minimum u_* in (10). Since the nighttime wind is relatively strong at Desert Rock (figure not shown), (10) is not needed. Therefore, results from N3 and N2 are essentially the same (Figs. 1a,b). At Gaize, the nighttime wind is weak, and the nighttime T_s results are slightly improved in N3 (Figs. 1c,d).

The N4 in Table 1 adds the constraint of minimum K_{soil} of 0.75 W m^{-1} K^{-1} to N3. This improves the overall

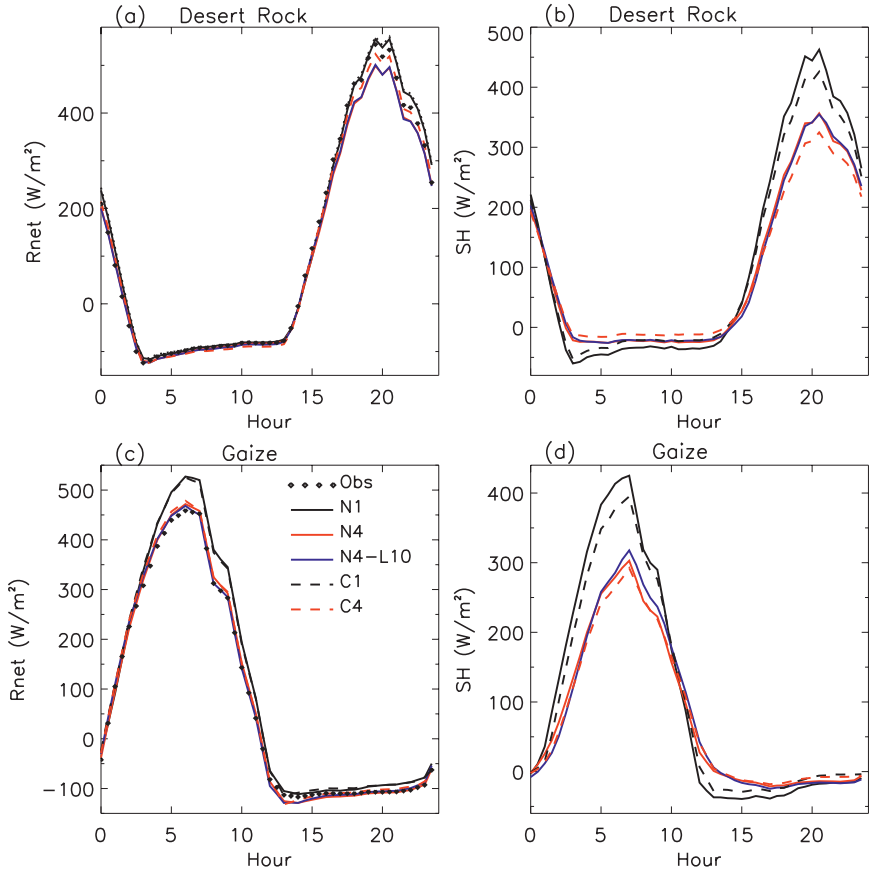

FIG. 3. (a) Observed and (CLM and Noah) simulated net radiative flux (R_{net}) and (b) SH flux over Desert Rock averaged from 3 to 31 Jul 2007. (c),(d) The corresponding results averaged from 18 days during 3–31 May 1998 over Gaize. Model sensitivity tests are explained in Table 1 and section 3b.

results at Desert Rock with the absolute bias within 1°C most of the time (Fig. 1b). At Gaize, the nighttime T_s results are further improved with the absolute bias within 2.5°C, while the daytime bias is slightly degraded.

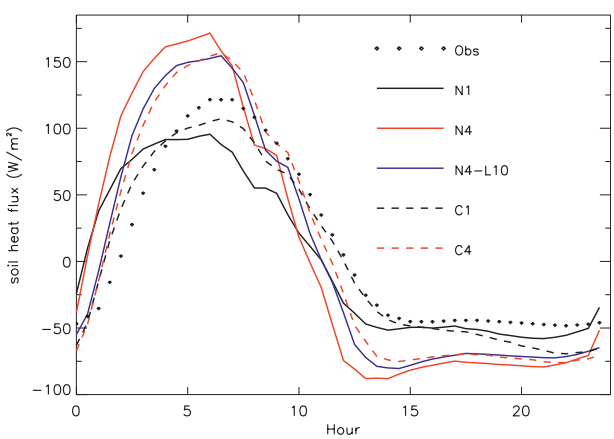

FIG. 4. The observed and (CLM and Noah) simulated soil heat flux at 0.025-m depth averaged from 18 days during 3–31 May 1998 over Gaize.

Compared with the control Noah simulation (N1), the mean absolute deviation in Fig. 1 is decreased from 2.8° to 0.5°C at Desert Rock and from 5.8° to 1.6°C at Gaize.

We also ran N4 with 10 soil layers (denoted as N4–L10 in Table 1). Results are very similar to those in N4 (Fig. 1), demonstrating the robustness of our improvements with respect to the number of vertical soil layers.

To further assess the robustness of our improvements, we have also run a different land model (CLM), and

TABLE 1. Summary of model experiments. The first letter N (or C) refers to Noah (or CLM), and more details of each experiment are provided in section 3b.

Noah Experiment	Description	CLM Experiment	Description
N0	Original Noah		
N1	N0 with $\text{iter}_{max} = 30$	C1	CLM control
N2	N1 with $a = 0.36$, $b = 0.5$	C2	C1 with $a = 0.36$, $b = 0.5$
N3	N2 + $u_{*\min}$	C3	C2 + $u_{*\min}$
N4	N3 + $K_{\text{soil,min}}$	C4	C3 + $K_{\text{soil,min}}$
N4–L10	N4 with 10 layers		

results are shown in Fig. 2. Similar to N1, the CLM control simulation (C1) significantly underestimates the maximum T_s at both sites. The nighttime T_s is underestimated to a lesser degree. The revisions in a and b in (9) (i.e., C2) largely remove the daytime underestimates and slightly improve the nighttime T_s. The constraint in the minimum u_* (C3) has a minimal effect at Desert Rock (Figs. 2a,b). At Gaize, it does not affect daytime T_s but slightly reduces nighttime T_s underestimate (Figs. 2c,d). The additional constraint of soil thermal conductivity (C4) improves the T_s simulation during the day but degrades the results at night at Desert Rock. In contrast, the results are improved at night but degraded during the day at Gaize. Compared with C1, C4 decreases the mean absolute deviation from 1.9° to 0.7°C at Desert Rock, and from 4.6° to 1.8°C at Gaize.

Figure 3 shows the changes of R_{net} and SH in sensitivity tests. The changes in G are not shown as they are very close to ($R_{\mathrm{net}} - \mathrm{SH}$). Both N1 and C1 overestimate R_{net} at Gaize, particularly in the early afternoon (Fig. 3c), because of the underestimate of T_s (Figs. 1d and 2d) [see Eq. (1)]. With our revisions, R_{net} is simulated very well in N4, C4, and N4–L10 at Gaize (Fig. 3c). At Desert Rock, C4 agrees with observed daytime R_{net} best (Fig. 3a), with N1 and C1 overestimating R_{net} while N4 and N4–L10 underestimate R_{net}. There are two reasons for the underestimate by N4 and N4–L10. First, a prescribed constant albedo (0.28) is used in Noah, while the observed albedo has a dependence on the solar zenith angle, with the albedo of about 0.27 near noon. This leads to an underestimate of about 10 W m^{-2} in R_{net} in N4 and N4–L10 near noon. Further, emissivity is taken as unity in Noah (versus about 0.93 from observations) in (1), which leads to an underestimate of about 25 W m^{-2} in R_{net}.

During the day, our revisions [particularly the increase of a in (9)] increase R_{ss} through (8) and hence decrease SH (Figs. 3b,d). Furthermore, this decrease is greater in magnitude than the decrease of R_{net}, leading to the increase of G (not shown). At night, the change of R_{net} is relatively small between sensitivity tests (e.g., between N1 and N4) (Figs. 3a,c), and our revisions (particularly the constraint of the minimum K_{soil}) increase the upward G in magnitude, leading to the decrease of SH in magnitude (Figs. 3b,d). The overall variation of SH is similar between N1 and C1, while the variation is similar among N4, N4–L10, and C4.

Ground heat flux was not measured at these two sites, but soil heat flux at 0.025-m depth was measured at Gaize. Figure 4 compares observed soil heat flux with the model results interpolated to this depth. The mean absolute deviations between N1, N4, N4–L10, C1, and C4 versus observed values in Fig. 4 are 24.2, 44.9, 31.1, 13.4, and 27.9 W m^{-2}, respectively. The model with 10 soil layers performs better than that with 4 layers (e.g., C4 and N4–L10 versus N4; C1 versus N1), partly because of a smaller discretization (or interpolation) error. Besides the horizontal representativeness issue of the soil heat flux measurements (e.g., Kustas et al. 2000), there are three additional reasons for our caution in interpreting these results in Fig. 4. First, to be consistent with the regional and global applications of Noah and CLM, we prescribe soil texture in our modeling rather than apply the soil thermal diffusivity computed from the observed soil heat flux and temporal variation of soil temperature as directly used in Yang et al. (2008) and Chen et al. (2010). With the exponential decrease of the soil heat flux diurnal amplitude with depth (e.g., Best et al. 2005), the model evaluation is sensitive to the measurement depth uncertainty. For instance, assuming the depth to be 0.03 m (rather than 0.025 m), the mean absolute deviation between N4–L10 versus observed values would be 21.7 W m^{-2} (rather than 31.1 W m^{-2}). Similarly, the linear interpolation of model fluxes to the measurement depth introduces uncertainties. As an example, we can compare the N4–L10 flux at 0.02-m depth with those interpolated from N4–L10 results at surface and 0.05-m depth, and the mean absolute deviation is 16.5 W m^{-2}.

c. *Discussion on global applications*

The implementation of our revisions in Noah and CLM is straightforward in the above offline simulations with the assumption of bare soil. For global applications, however, we have to consider the characterization of vegetation and other model details.

Since CLM uses subgrid tiles (including bare soil) based on the annually maximum fractional vegetation cover along with seasonally variable leaf-area index (LAI) for each vegetation type (Oleson et al. 2010), (9) with the new a and b values can be directly used over the bare soil tile. Furthermore, since z_{om} is used in (9), the convergence of z_{om} under sparse and dense canopy conditions needs to be considered (Zeng and Wang 2007). A related issue—that is, the convergence of undercanopy turbulence for thick and thin canopies in CLM and other land models—is also important (Zeng et al. 2005).

In contrast to CLM, Noah does not consider subgrid tiles; that is, bare soil and vegetated area are treated together based on seasonally variable green vegetation fraction (GVF) along with a constant LAI (Mitchell et al. 2004). Therefore, the convergence of z_{om} under small and large GVF conditions needs to be considered (Zheng et al. 2012). For instance, for the NCEP GFS grid cell covering the Desert Rock site, z_{om} is 0.158 m, because this grid cell is classified as shrubs (but with

a very small GVF). It converges to the more appropriate value of about 0.01 m after computing the effective z_{om} in Zheng et al. (2012) [i.e., using (11) below].

Traditionally, the same value of a (or $0.4C_{zil}$) was used in Noah, independent of vegetation type or GVF (LeMone et al. 2008). For instance, C_{zil} was taken as 0.2 in the earlier version of Noah, 0.1 in the Noah version used in WRF, and 0.0 in GFS before May 2011. Since May 2011, GFS has implemented C_{zil} of 0.8 (or $a = 0.32$) along with (11) below (Zheng et al. 2012).

As discussed in Zeng and Dickinson (1998), different values of z_{om} and z_{oh} are needed over bare soil only, as energy balance is explicitly considered over canopy, which is equivalent to the consideration of z_{om}/z_{oh}. Since a single temperature is used for canopy and ground in Noah, (9) can be modified for global applications (Zheng et al. 2012):

$$\ln(z_{om,e}/z_{oh}) = (1-\mathrm{GVF})^2 a\left(\frac{u_* z_{og}}{\nu}\right)^b, \qquad (11)$$

where $z_{om,e}$ refers to the effective z_{om} discussed above, and z_{og} is the bare soil roughness length (0.01 m in both CLM and Noah). While this formulation has been tested in the land–atmosphere coupled GFS in Zheng et al. (2012), further efforts are needed to address the impact of these revised a and b values on global CLM modeling.

Alternatively, C_{zil} is computed from $C_{zil} = 10^{-0.4h}$ with h being the canopy height in Chen and Zhang (2009). For a forest grid cell with a high GVF, a converges to the correct value of zero from both this formulation and (11). For a model grid cell over arid shrubland with GVF = 0.05 and $z_{om} = 0.1$ m (for shrubs), the results (with 95% bare soil) should be similar to those over 100% bare soil. This is the case for (11) as $(1 - \mathrm{GVF})^2 a = 0.9 \times 0.9 = 0.81$. In contrast, $C_{zil} = 0.4$ (or $a = 0.16$) from Chen and Zhang (2009), which is very different from the bare soil value of a (0.9). Further efforts are needed for a detailed comparison of these formulations over grid cells with different GVF values in Noah.

The z_{oh} formulation of Yang et al. (2008) does not depend on z_{om} and yields results similar to those based on $a = 0.9$ in the turbulence computation over bare soil, as mentioned in section 2b. However, it is unclear how it should be used over grid cells with different GVF values.

The minimum u_* in (10) considers the dependence on elevation and vegetation type. For CLM, it can be directly used over bare soil and vegetated subgrid tiles. For Noah, it can be used if z_{om} is replaced by its effective value ($z_{om,e}$) over a model grid cell. Future efforts are needed to evaluate the impact of (10) over vegetated grid cells.

The constraint of the minimum K_{soil} in the computation of G can be directly used in CLM and Noah. It is not needed (i.e., K_{soil} would be greater than $K_{soil,min}$) when the soil is not too dry. For instance, for sandy clay soil in Noah, the wilting point volumetric soil moisture is 0.1, and the corresponding K_{soil} is 0.86 W m^{-1} K^{-1}, which is greater than $K_{soil,min}$ of 0.75 W m^{-1} K^{-1}. Because K_{soil} is modified by GVF in Noah (LeMone et al. 2008), the above constraint should be applied before this modification in Noah. Again, future efforts are still needed to evaluate the impact of this constraint over vegetated grid cells.

4. Conclusions

Three revisions are proposed to significantly improve the land surface modeling of the diurnal cycle of surface skin temperature (T_s) over arid regions using Noah and CLM. The revision of the coefficients a (or $0.4C_{zil}$) in the computation of roughness length for heat in (9) or (11) is most effective in reducing the daytime T_s underestimate, while the constraints of the minimum friction velocity u_* and soil thermal conductivity help reduce the nighttime T_s underestimate under weak wind and dry soil conditions. These results are robust with respect to two different community land models (Noah and CLM) or the same model (Noah) with 4 versus 10 soil layers. Furthermore, model improvements are consistent at the Desert Rock site in Nevada with a monthly averaged diurnal amplitude of 31.7°C and at the Gaize site in Tibet, China, with an amplitude of 44.6°C. Therefore, these revisions in Noah and CLM are very probably applicable to global arid regions. The global testing of the first revision in GFS/Noah has been done and the positive impact of this revision on weather forecasting and satellite data assimilation over arid regions was reported in Zheng et al. (2012). The global testing of other two revisions in GFS/Noah and of all three revisions in CLM (or global atmospheric model coupled with CLM) remains to be done. These revisions may also be applicable to other land models over global arid regions, but actual tests remain to be done.

Our revisions can be directly applied to CLM or other land models with subgrid tiles (including bare soil). In contrast, for Noah and other land models without subgrid tiles (i.e., treating bare soil and vegetated area together in each grid cell), care must be taken in the implementations. For instance, effective roughness length for momentum needs to be computed, and the green vegetation fraction needs to be considered in the computation of roughness length for heat as provided in (11).

Traditionally, C_{zil} (or $a = 0.4C_{zil}$) has been taken as a fully tunable parameter in Noah. For instance, C_{zil} was taken as 0.2 in the earlier version of Noah, 0.1 in WRF/Noah, and 0.0 in GFS/Noah, independent of green

vegetation fraction (GVF) or vegetation type. Many more different values of C_{zil} were used by Noah users. Zeng and Dickinson (1998) emphasized that a nonzero a (or C_{zil}) is needed over bare soil only. It is hoped that the value of a (0.9) determined from this study, or a small range of values around 0.9, along with the explicit consideration of GVF in (11) will be used by Noah users in the future. This approach was operationally implemented in GFS/Noah in May 2011. Alternatively, the vegetation type–dependent formulation for C_{zil} from Chen and Zhang (2009) could be used. In other words, if Noah simulations are deficient, the users should improve other parts of the model, rather than arbitrarily adjust the coefficient a (or C_{zil}).

Under very stable (atmospheric stratification) conditions, it is a challenging task to measure or simulate the surface sensible heat flux (because of turbulence, intermittency, and other processes). This study provides a new perspective in addressing this issue: we should not take the surface sensible heat flux computation or measurement under stable conditions as an atmospheric turbulence issue alone; instead, we should address it as a land–atmosphere coupled issue. Over arid regions this involves the interplay of ground heat flux and sensible heat flux in balancing the net radiation. If a land model can reproduce the observed net radiation, surface skin temperature, and, to a lesser degree, soil heat flux (e.g., at 0.025-m depth) at an arid site, can we use the computed sensible heat flux to infer the true flux? For instance, the nighttime downward sensible heat fluxes would be 10–20 W m^{-2} at both sites (Figs. 3b,d). Such values under stable conditions represent different constraints from those due to atmospheric boundary layer turbulence [e.g., because of large eddies under weak wind and unstable conditions (Zeng et al. 1998)]. From this coupling perspective, two relevant questions can be raised here for the measurement and modeling communities. For land–atmosphere coupled modeling, how do our constraints of minimum u_* and soil thermal conductivity affect the stable atmospheric boundary layer and its coupling with land processes? A similar issue—that is, the impact of soil moisture freezing on the stable atmospheric boundary layer—was addressed in Viterbo et al. (1999). For eddy-correlation flux measurements, the question raised is: Can we use $u_{*\min}$ in (10) to identify the periods over any land cover type or at any elevation when the underestimation of flux may occur?

Because the maximum iteration number is set to be five in the turbulence computation in Noah, the computation does not converge under very stable conditions. This would probably affect all offline Noah simulations over arid regions. Further analysis is needed to assess the relevance of this issue to atmosphere–land coupled modeling (e.g., WRF/Noah and GFS/Noah). A simple solution is to increase the maximum iteration number from 5 to 30 (in offline Noah modeling), similar to our finding under snow conditions (Wang et al. 2010).

Acknowledgments. This work was supported by NOAA (NA10NES4400006), NASA (NNX09A021G), and NSF grants (AGS-0944101). Peggy LeMone and Ethan Gutmann are thanked for very carefully reading our manuscript and providing helpful comments/suggestions. Data at Gaize were obtained from the Coordinated Enhanced Observing Period (CEOP) Asian Monsoon Project (CAMP/Tibet), while data at Desert Rock were obtained from the NOAA Surface Radiation (SURFRAD) Network.

REFERENCES

Baklanov, A. A., and Coauthors, 2011: The nature, theory, and modeling of atmospheric planetary boundary layers. *Bull. Amer. Meteor. Soc.,* **92,** 123–128.

Baldocchi, D., and Coauthors, 2001: FLUXNET: A new tool to study the temporal and spatial variability of ecosystem-scale carbon dioxide, water vapor, and energy flux densities. *Bull. Amer. Meteor. Soc.,* **82,** 2415–2434.

Beljaars, A. C. M., and P. Viterbo, 1998: Role of the boundary layer in a numerical weather prediction model. *Clear and Cloudy Boundary Layers,* A. A. M. Holtslag and P. G. Duynkerke, Eds., Royal Netherlands Academy of Arts and Sciences, 287–304.

Best, M. J., P. M. Cox, and D. Warrilow, 2005: Determining the optimal soil temperature scheme for atmospheric modeling applications. *Bound.-Layer Meteor.,* **114,** 111–142.

Chen, F., and J. Dudhia, 2001: Coupling an advanced land surface–hydrology model with the Penn State–NCAR MM5 modeling system. Part I: Model implementation and sensitivity. *Mon. Wea. Rev.,* **129,** 569–585.

——, and Y. Zhang, 2009: On the coupling strength between the land surface and the atmosphere: From viewpoint of surface exchange coefficients. *Geophys. Res. Lett.,* **36,** L10404, doi:10.1029/2009GL037980.

Chen, Y., K. Yang, D. Zhou, J. Qin, and X. Guo, 2010: Improving the Noah land surface model in arid regions with an appropriate parameterization of the thermal roughness length. *J. Hydrometeor.,* **11,** 995–1006.

Decker, M., M. Brunke, Z. Wang, K. Sakaguchi, X. Zeng, and M. G. Bosilovich, 2012: Evaluation of the reanalysis products from GSFC, NCEP, and ECMWF using flux tower observations. *J. Climate,* **25,** 1916–1944.

Ek, M. B., K. E. Mitchell, Y. Lin, E. Rogers, P. Grunmann, V. Koren, G. Gayno, and J. D. Tarpley, 2003: Implementation of Noah land surface model advances in the National Centers for Environmental Prediction operational mesoscale Eta model. *J. Geophys. Res.,* **108,** 8851, doi:10.1029/2002JD003296.

Fernando, H. J. S., and J. C. Weil, 2010: Whither the stable boundary layer? A shift in the research agenda. *Bull. Amer. Meteor. Soc.,* **91,** 1475–1484.

Garratt, J. R., 1992: *The Atmospheric Boundary Layer*. Cambridge University Press, 316 pp.

Goulden, M. L., J. W. Munger, S.-M. Fan, B. C. Daube, and S. C. Wofsy, 1996: Measurements of carbon sequestration by long-term eddy covariance: Methods and a critical evaluation of accuracy. *Global Change Biol.,* **2,** 169–182.

Gu, L., and Coauthors, 2005: Objective threshold determination for nighttime eddy flux filtering. *Agric. For. Meteor.,* **128,** 179–197.

Gutmann, E. D., and E. E. Small, 2007: A comparison of land surface model soil hydraulic properties estimated by inverse modeling and pedotransfer functions. *Water Resour. Res.,* **43,** W05418, doi:10.1029/2006WR005135.

Jiménez, C., and Coauthors, 2011: Global intercomparison of 12 land surface heat flux estimates. *J. Geophys. Res.,* **116,** D02102, doi:10.1029/2010JD014545.

Jin, M., R. E. Dickinson, and A. M. Vogelmann, 1997: A comparison of CCM2–BATS skin temperature and surface–air temperature with satellite and surface observations. *J. Climate,* **10,** 1505–1524.

Kabat, P., and Coauthors, 2004: *Vegetation, Water, Humans and the Climate: A New Perspective on an Interactive System*. Global Change: The IGBP Series, Vol. 24, Springer Verlag, 566 pp.

Koster, R. D., and Coauthors, 2006: GLACE: The Global Land–Atmosphere Coupling Experiment. Part I: Overview. *J. Hydrometeor.,* **7,** 590–610.

Kustas, W. P., J. H. Prueger, J. L. Hatfield, K. Ramalingam, and L. E. Hipps, 2000: Variability in soil heat flux from a mesquite dune site. *Agric. For. Meteor.,* **103,** 249–264.

LeMone, M. A., M. Tewari, F. Chen, J. Alfieri, and D. Niyogi, 2008: Evaluation of the Noah land surface model using data from a fair-weather IHOP_2000 day with heterogeneous surface fluxes. *Mon. Wea. Rev.,* **136,** 4915–4941.

Mahrt, L., 2010: Variability and maintenance of turbulence in the very stable boundary layer. *Bound.-Layer Meteor.,* **135,** 1–18, doi:10.1007/s10546-009-9463-6.

Mitchell, K., and Coauthors, 2004: The multi-institution North American Land Data Assimilation System (NLDAS): Utilizing multiple GCIP products and partners in a continental distributed hydrological modeling system. *J. Geophys. Res.,* **109,** D07S90, doi:10.1029/2003JD003823.

Oleson, K. W., and Coauthors, 2008: Improvements to the Community Land Model and their impact on the hydrological cycle. *J. Geophys. Res.,* **113,** G01021, doi:10.1029/2007JG000563.

——, and Coauthors, 2010: Technical description of version 4.0 of the Community Land Model (CLM). NCAR Tech. Note NCAR/TN-478+STR, 257 pp.

Reichle, R. H., S. V. Kumar, S. P. P. Mahanama, R. D. Koster, and Q. Liu, 2010: Assimilation of satellite-derived skin temperature observations into land surface models. *J. Hydrometeor.,* **11,** 1103–1122.

Sellers, P. J., and Coauthors, 1997: Modeling the exchanges of energy, water, and carbon between continents and the atmosphere. *Science,* **275,** 502–509.

Seneviratne, S. I., D. Lathi, M. Litschi, and C. Schar, 2006: Land–atmosphere coupling and climate change in Europe. *Nature,* **443,** 205–209.

Shuttleworth, W. J., 2011: *Terrestrial Hydroclimatology*. Wiley-Blackwell, 560 pp.

Viterbo, P., A. Beljaars, J.-F. Mahfouf, and J. Teixeira, 1999: The representation of soil moisture freezing and its impact on the stable boundary layer. *Quart. J. Roy. Meteor. Soc.,* **125,** 2401–2426.

Wang, Z., M. Barlage, X. Zeng, R. E. Dickinson, and C. B. Schaaf, 2005: The solar zenith angle dependence of desert albedo. *Geophys. Res. Lett.,* **32,** L05403, doi:10.1029/2004GL021835.

——, X. Zeng, and M. Decker, 2010: Improving snow processes in the Noah land model. *J. Geophys. Res.,* **115,** D20108, doi:10.1029/2009JD013761.

Xue, Y., F. De Sales, R. Vasic, C. R. Mechoso, S. D. Prince, and A. Arakawa, 2010: Global and temporal characteristics of seasonal climate/vegetation biophysical process (VBP) interactions. *J. Climate,* **23,** 1411–1433.

Yang, K., and Coauthors, 2008: Turbulent flux transfer over bare-soil surfaces: Characteristics and parameterization. *J. Appl. Meteor. Climatol.,* **47,** 276–290.

Zheng, W., H. Wei, Z. Wang, X. Zeng, J. Meng, M. Ek, K. Mitchell, and J. Derber, 2012: Improvement of daytime land surface skin temperature over arid regions in the NCEP GFS model and its impact on satellite data assimilation. *J. Geophys. Res.,* **117,** D06117, doi:10.1029/2011JD015901.

Zeng, X., and R. E. Dickinson, 1998: Effect of surface sublayer on surface skin temperature and fluxes. *J. Climate,* **11,** 537–550.

——, and A. Wang, 2007: Consistent parameterization of roughness length and displacement height for sparse and dense canopies in land models. *J. Hydrometeor.,* **8,** 730–737.

——, M. Zhao, and R. E. Dickinson, 1998: Intercomparison of bulk aerodynamic algorithms for the computation of sea surface fluxes using the TOGA COARE and TAO data. *J. Climate,* **11,** 2628–2644.

——, M. Shaikh, Y. Dai, R. E. Dickinson, and R. Myneni, 2002: Coupling of the Common Land Model to the NCAR Community Climate Model. *J. Climate,* **15,** 1832–1854.

——, R. E. Dickinson, M. Barlage, Y. Dai, G. Wang, and K. Oleson, 2005: Treatment of under-canopy turbulence in land models. *J. Climate,* **18,** 5086–5094.